


Plasmons and screening in finite-bandwidth two-dimensional electron gas

Kaveh Khaliji,¹ Tobias Stauber,² and Tony Low^{1,*}

¹*Department of Electrical and Computer Engineering, University of Minnesota, Minneapolis, Minnesota 55455, USA*

²*Materials Science Factory, Instituto de Ciencias de Materiales de Madrid, CSIC, E-28049 Madrid, Spain*

 (Received 4 October 2019; revised 24 June 2020; accepted 13 August 2020; published 8 September 2020)

The dynamical and nonlocal dielectric function of a two-dimensional electron gas with finite-energy bandwidth is computed within a random-phase approximation. For large bandwidth, the plasmon dispersion has two separate branches at small and large momenta. The large-momenta branch exhibits negative quasiflat dispersion. The two branches merge with decreasing bandwidth. We discuss how the maximum-energy plasmon mode, which resides at energies larger than all particle-hole continuum, can potentially open a route to low-loss plasmons. Moreover, we discuss the bandwidth effects on the static screening of the charged and magnetic impurities.

DOI: [10.1103/PhysRevB.102.125408](https://doi.org/10.1103/PhysRevB.102.125408)

I. INTRODUCTION

Since the early 1950s, there has been ongoing interest in the theory of two-dimensional (2D) electronic systems. This has been partly fueled by the development of metal-oxide-semiconductor transistors, where the surface-accumulated charge layers formed in the device behave as a two-dimensional electron gas (2DEG) [1–3]. The isolation of atomically thin layers from bulk parent materials [4] has also boosted this interest, where the theory of 2DEG has served as a point of reference for the elementary electronic properties of graphene and other 2D systems [5–9].

The dynamical 2D polarizability, which describes the screening of the Coulomb potential, is vital for understanding many physical properties in 2D systems. For example, dynamical screening governs the elementary excitation spectra and gives the collective modes dispersion. Moreover, in a noninteracting 2D electron gas without spin-orbit coupling, the static screening dictates the magnetic response via control over exchange interactions between localized magnetic impurities embedded in the 2D metal, or determines the transport properties through screened Coulomb scattering by charged impurities [10,11].

With the 2DEG polarizability now a textbook example covered in many-body physics [10], we ask a seemingly simple question: how does the polarizability function get modified if we restrict the parabolic energy dispersion with an energy cutoff? This was motivated by recent developments in several materials system exhibiting isolated electronic bands with finite bandwidths. This includes TaS₂ or NbS₂ single layers in the 2H phase [12], or Si(111):X in the $\alpha - \sqrt{3} \times \sqrt{3}$ phase, constructed by group-IV adatom X adsorbed on a silicon surface (111) [13–15]. We show that a finite bandwidth allows for plasmon modes of quasiflat dispersion and large momenta to emerge. The finite-bandwidth 2DEG (FBW-2DEG) can also potentially support low-loss plasmon modes that

are immune to elastic or inelastic scattering-assisted Landau damping (dissipation via electron-hole pair excitation). We show that the static polarizability approaches a constant value at the large-momenta limit and the value can be tuned with bandwidth and Fermi energy. We find, in FBW-2DEG, that static Friedel oscillations due to a charged impurity can be strongly damped as the bandwidth shrinks. However, the induced spin density due to a magnetic impurity has a large-distance oscillatory decay similar to the 2DEG, and is not affected by the bandwidth.

II. DYNAMIC POLARIZABILITY AND PLASMON MODES

We assume an electronic energy dispersion of the form $E_{\mathbf{k}} = \hbar^2 k^2 / 2m$ for $k \leq k_c$, and $E_{\mathbf{k}} = E_c$ otherwise. The Fermi energy and momentum are denoted with E_F and k_F , respectively. Accordingly, we introduce $\bar{E}_c = E_c / E_F$ and $\bar{k}_c = k_c / k_F$. In Fig. 1, the main symbols pertaining to FBW-2DEG electron energy dispersion are illustrated. In this work, we assume $\bar{k}_c > 1$.

The dielectric function in the random-phase approximation reads

$$\epsilon(\mathbf{q}, \omega) = 1 + \frac{e^2}{2\epsilon_0 \kappa q} P(\mathbf{q}, \omega), \quad (1)$$

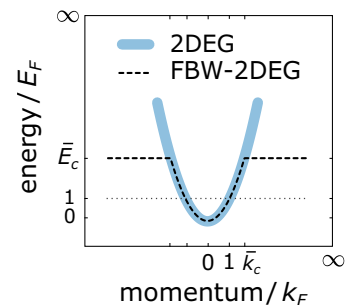


FIG. 1. The 2DEG and FBW-2DEG electron energy dispersions. The dotted line is the Fermi energy.

*tlow@umn.edu

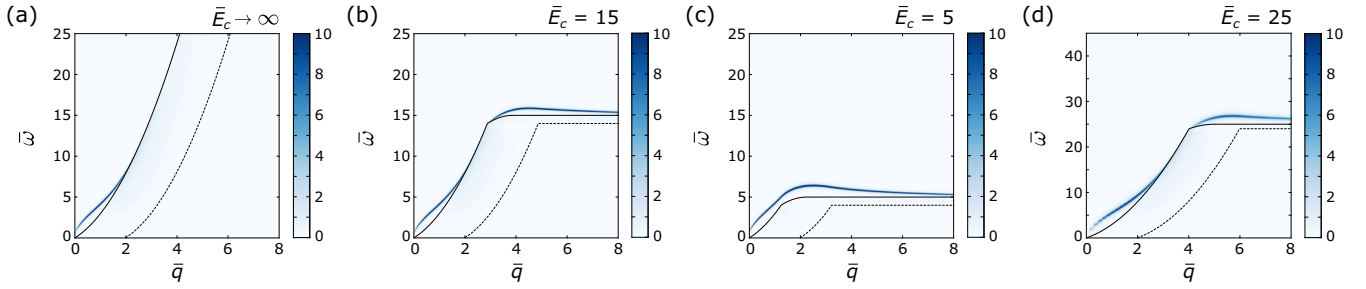


FIG. 2. The loss function for (a) 2DEG, (b) $E_c = 1.5$ eV, and (c) $E_c = 0.5$ eV, all at a fixed $E_F = 0.1$ eV. (d) The same as (c), for $E_F = 0.02$ eV. The solid and dashed black lines denote upper and lower boundaries of the PHC, respectively. $\eta = 5$ meV is assumed.

with the Lindhard polarizability given as

$$P(\mathbf{q}, \omega) = -\frac{2}{S} \sum_{\mathbf{k}} \frac{f_{\mathbf{k}} - f_{\mathbf{k}+\mathbf{q}}}{E_{\mathbf{k}} - E_{\mathbf{k}+\mathbf{q}} + \hbar\omega + i\eta}, \quad (2)$$

where S is the sample area and κ is the background dielectric constant. We use $m/m_0 = 0.5$, $E_F = 0.1$ eV, and $\kappa = 2.5$, unless denoted otherwise. We assume zero temperature. The undamped plasmon modes correspond to zeros of the dielectric function. For finite broadening, where $\text{Im } P \neq 0$, the loss function, defined as $L(\mathbf{q}, \omega) = -\text{Im} [1/\epsilon(\mathbf{q}, \omega)]$, is used to visualize the low-loss plasmon modes which appear as sharp peaks [16].

For 2DEG, i.e., when $E_c \rightarrow \infty$, the plasmon dispersion has the analytic form ($\eta \rightarrow 0$) [17]:

$$\bar{\omega}^2 = 2\bar{q}_{\text{TF}}\bar{q} \left(1 + \frac{\bar{q}}{\bar{q}_{\text{TF}}}\right)^2 \left(1 + \frac{\bar{q}^3}{2\bar{q}_{\text{TF}}^3} + \frac{\bar{q}^4}{4\bar{q}_{\text{TF}}^4}\right) / \left(1 + \frac{\bar{q}}{2\bar{q}_{\text{TF}}}\right), \quad (3)$$

where $\bar{\omega} = \hbar\omega/E_F$, $\bar{q} = q/k_F$, $\bar{q}_{\text{TF}} = q_{\text{TF}}/k_F$, and $q_{\text{TF}} = me^2/2\pi\hbar^2\kappa\epsilon_0$ is the Thomas-Fermi wave vector for the 2DEG. We note that Eq. (3) gives a valid description for $q \leq q_c$, the critical wave vector at which the plasmon mode touches the 2DEG particle-hole continuum (PHC). The plasmon dispersion ceases to exist for $q > q_c$ [see Fig. 2(a)]. This critical wave vector can be determined via [17]

$$\frac{\bar{q}_c^2}{\bar{q}_{\text{TF}}} + \frac{\bar{q}_c^3}{2\bar{q}_{\text{TF}}^2} = 1, \quad (4)$$

where $\bar{q}_c = q_c/k_F$.

When a cutoff is introduced, two changes are evident [see Fig. 2(b)]: (1) The PHC is reconfigured, and the maximum energy for single-particle transitions is now limited by the bandwidth. (2) In addition to *low-q* plasmon modes which resemble the plasmons in 2DEG, another plasmon branch appears at *large q*, with energies close to E_c . With decreasing bandwidth, the two branches merge; see Fig. 2(c). We note that decreasing E_F at a given bandwidth has a similar effect as increasing bandwidth at a fixed E_F , i.e., we start with one branch which evolves into two separate branches at smaller E_F ; see Figs. 2(c) and 2(d).

These trends can be followed via a semianalytical model, valid for a clean sample ($\eta \rightarrow 0$) at zero temperature. The model is built upon the following argument: in Eq. (2), for $q \leq k_c - k_F$, $E_{\mathbf{k}+\mathbf{q}} = \hbar^2|\mathbf{k} + \mathbf{q}|^2/2m$ and the polarizability is

identical to that of a 2DEG. For $q \geq k_c + k_F$, we have $E_{\mathbf{k}+\mathbf{q}} = E_c$. For $k_c - k_F \leq q \leq k_c$, $E_{\mathbf{k}+\mathbf{q}} = E_c$ only if $k_c - q \leq k \leq k_F$ and $0 \leq \theta \leq \theta_0$, where θ is the angle between \mathbf{k} and \mathbf{q} , and

$$\theta_0 = \cos^{-1} \left(\frac{k_c^2 - k^2 - q^2}{2kq} \right) \quad (5)$$

is the angle at which $|\mathbf{k} + \mathbf{q}| = k_c$. Likewise, for $k_c \leq q \leq k_c + k_F$, $E_{\mathbf{k}+\mathbf{q}} = \hbar^2|\mathbf{k} + \mathbf{q}|^2/2m$, only if $q - k_c \leq k \leq k_F$ and $\theta_0 \leq \theta \leq \pi$. Accordingly, the closed-form relations for the imaginary part of the polarizability, within different phase space defined in Fig. 3(a), can be obtained as

$$\text{Im } P(\bar{q}, \bar{\omega}) = \frac{m}{2\pi\hbar^2} \frac{1}{\bar{q}^2} [\sqrt{4\bar{q}^2 - (\bar{\omega} - \bar{q}^2)^2} - \sqrt{4\bar{q}^2 - (\bar{\omega} + \bar{q}^2)^2}] \quad (6a)$$

in region i: $0 \leq \bar{\omega} \leq \min\{-(\bar{q} - 1)^2 + 1, \bar{E}_c - 1\}$;

$$\text{Im } P(\bar{q}, \bar{\omega}) = \frac{m}{2\pi\hbar^2} \frac{1}{\bar{q}^2} \sqrt{4\bar{q}^2 - (\bar{\omega} - \bar{q}^2)^2} \quad (6b)$$

in region ii: $\max\{-(\bar{q} - 1)^2 + 1, (\bar{q} - 1)^2 - 1\} \leq \bar{\omega} \leq \min\{(\bar{q} + 1)^2 - 1, \bar{E}_c - 1\}$;

$$\text{Im } P(\bar{q}, \bar{\omega}) = \frac{m}{2\pi\hbar^2} \frac{1}{\bar{q}^2} [\sqrt{4(\bar{E}_c - \bar{\omega})\bar{q}^2 - (\bar{\omega} - \bar{q}^2)^2} - \sqrt{4\bar{q}^2 - (\bar{\omega} + \bar{q}^2)^2}] + \frac{m}{\pi\hbar^2} \cos^{-1} \left(\frac{\bar{\omega} - \bar{q}^2}{2\bar{q}\sqrt{\bar{E}_c - \bar{\omega}}} \right) \quad (6c)$$

in region iii: $\bar{E}_c - 1 \leq \bar{\omega} \leq -(\bar{q} - 1)^2 + 1$ (note that this region appears only if $\bar{k}_c \leq \sqrt{2}$);

$$\text{Im } P(\bar{q}, \bar{\omega}) = \frac{m}{2\pi\hbar^2} \frac{1}{\bar{q}^2} \sqrt{4(\bar{E}_c - \bar{\omega})\bar{q}^2 - (\bar{\omega} - \bar{q}^2)^2} + \frac{m}{\pi\hbar^2} \cos^{-1} \left(\frac{\bar{\omega} - \bar{q}^2}{2\bar{q}\sqrt{\bar{E}_c - \bar{\omega}}} \right) \quad (6d)$$

in region iv: $\max\{-(\bar{q} - 1)^2 + 1, \bar{E}_c - 1\} \leq \bar{\omega} \leq \bar{E}_c - (\bar{q} - \bar{k}_c)^2$; and

$$\text{Im } P(\bar{q}, \bar{\omega}) = \frac{m}{\hbar^2} \quad (6e)$$

in region v: $\bar{q} \geq \bar{k}_c$ and $\max\{\bar{E}_c - (\bar{q} - \bar{k}_c)^2, \bar{E}_c - 1\} \leq \bar{\omega} \leq \bar{E}_c$. We then use Kramers-Kronig transformation to obtain the real part of the polarizability. In Fig. 3(a), the boundaries

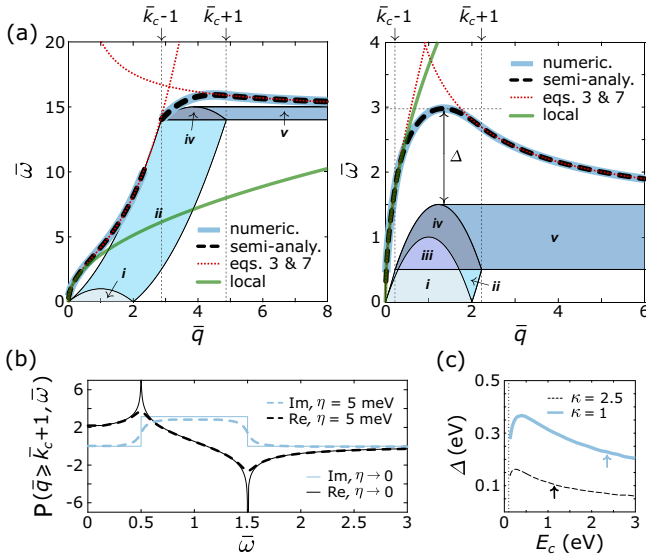


FIG. 3. (a) The plasmon dispersions obtained numerically (exact) and via semi-analytic model. The dispersions obtained via Eqs. (3) and (7), and via local model ($\bar{\omega} = \sqrt{2\bar{q}\bar{q}_{\text{TF}}}$), are also plotted. The different regions characterizing the $\text{Im} P \neq 0$ are also displayed. The left panel: $\bar{E}_c = 15$. The right panel: $\bar{E}_c = 1.5$. (b) The real and imaginary parts of the polarizability (normalized to $m/\pi\hbar^2$) for zero and 5 meV broadening at $\bar{q} \geq \bar{k}_c + 1$ and $\bar{E}_c = 1.5$. (c) Δ vs bandwidth. The dotted line is the Fermi energy. The arrows denote the bandwidth at which merging occurs.

of the PHC are illustrated. The plasmon dispersion obtained from this semianalytic method compares well with the numeric result.

We note that Eq. (3) also gives the plasmon modes in FBW-2DEG for $\bar{q} \leq \min\{\bar{q}_c, \bar{k}_c - 1\}$ [see Fig. 3(a)]. The bandwidth at which the two plasmon branches merge can be followed via $\bar{k}_c \sim \bar{q}_c + 1$. The latter is the condition for the *low-q* plasmon branch to jump over the PHC at $\bar{q} = \bar{k}_c - 1$. We note that the E_c required for merging increases with the Fermi level and decreases with κ .

For $\bar{q} \geq \bar{k}_c + 1$, a closed-form expression can be obtained for the plasmon dispersion in FBW-2DEG [see Fig. 3(a)],

$$\bar{\omega}^2 = \frac{2\bar{E}_c - 1}{\exp(\bar{q}/\bar{q}_{\text{TF}}) - 1} + \bar{E}_c^2. \quad (7)$$

Interestingly, although the plasmon energy is asymptotically approaching \bar{E}_c for $\bar{q} \gg \bar{k}_c + 1$, at zero temperature and $\eta \rightarrow 0$, it does not enter the PHC. This can be tracked by inspecting the real part of the polarizability for $\bar{q} \geq \bar{k}_c + 1$, which reads

$$\text{Re} P(\bar{q}, \bar{\omega}) = \frac{m}{\pi\hbar^2} \ln \left[\frac{\bar{E}_c^2 - \bar{\omega}^2}{(\bar{E}_c - 1)^2 - \bar{\omega}^2} \right]. \quad (8)$$

It is clear that the latter becomes singular at $\bar{\omega} = \bar{E}_c$, which guarantees a zero for the dielectric function, irrespective of the \bar{q} magnitude. This, however, can be relaxed for a finite broadening, as illustrated in Fig. 3(b). For a 2D system sandwiched between two dielectric mediums, the plasmon momentum is inversely proportional to the field decay length. This suggests unprecedented field confinement in FBW-2DEG.

Moreover, for $q \gtrsim q_{\text{TF}} \ln(E_F/\Delta E)$, the plasmon energy varies in the range ΔE above E_c , which allows for plasmon modes with almost constant dispersion to emerge. The onset q for this quasiflat dispersion can also be tuned with the dielectric choice or Fermi energy. This allows for tunable near-field exponential amplification in a setup which has two FBW-2DEGs separated by a dielectric spacer [18,19].

We next focus on the plasmon mode with maximum energy, where we introduce Δ , denoting its energy relative to the upper boundary of the PHC; see Fig. 3(a). The importance of this mode is twofold: (1) Low-loss plasmon. This mode is arguably protected against Landau damping mediated by elastic scattering since pure momentum transfer will not be adequate to bring it into the PHC. Moreover, given $\Delta \gg E_c$, damping pathways due to optical phonon inelastic scattering are also quenched. In Fig. 3(c), we show, in FBW-2DEG, that dielectric engineering is a plausible route to protect maximum-energy plasmons against both elastic and inelastic scattering-mediated Landau damping. Also note that Δ vs bandwidth has a maximum which occurs at E_c , well below the bandwidth required for merging and larger than Fermi energy. (2) Negative group velocity. We note that the group velocity changes sign at the momentum pertaining to the maximum-energy plasmon. This mode occurs at $q \sim k_c$, which implies that the onset for negative dispersion can be tuned via controlling the bandwidth. The tunability of the group velocity sign allows for interesting phenomena such as all-angle negative refraction, normal Doppler frequency shift, or tunable directional plasmon excitation [20–23].

We note that the idea to achieve lossless plasmons in narrowband electronic systems has been explored in the context of bulk metals via computing the local dielectric function [12,24]. The local description, by definition, assumes identical loss for all momenta and gives an incomplete view of the PHC boundaries. It thus cannot be used to predict the mode robustness against Landau damping, an intrinsic and major damping channel in 2D metals [25]. In addition to loss, the local description cannot correctly account for the features that arise in the dispersion. In the local limit, $q \rightarrow 0$ and for a clean sample, the polarizability for the FBW is identical to that of 2DEG. The zeros of the local dielectric function, which give the local plasmon dispersion are thus given as $\bar{\omega} = \sqrt{2\bar{q}\bar{q}_{\text{TF}}}$. The latter expression clearly gives no information of the large- q branch, its merging with the low- q branch, or the maximum-energy plasmon modes; see Fig. 3(a). These points suggest that the nonlocal model is a prerequisite to explain the lossless plasmon that can emerge in FBW 2D metals.

III. STATIC SCREENING AND FRIEDEL OSCILLATIONS

The static limit of the polarizability, $\omega = 0$ with arbitrary q , is relevant for the screening of charged and magnetic impurities. In Fig. 4(a), we cover this limit. For a 2DEG with $E_c \rightarrow \infty$, the static polarizability is given by [26]

$$P(\bar{q}, 0) = \frac{m}{\pi\hbar^2} \left[1 - \theta(\bar{q} - 2) \sqrt{1 - \frac{4}{\bar{q}^2}} \right]. \quad (9)$$

This is also valid for FBW-2DEG given that $\bar{q} \leq \bar{k}_c - 1$. For 2DEG at a short-wavelength limit, the static polarizability

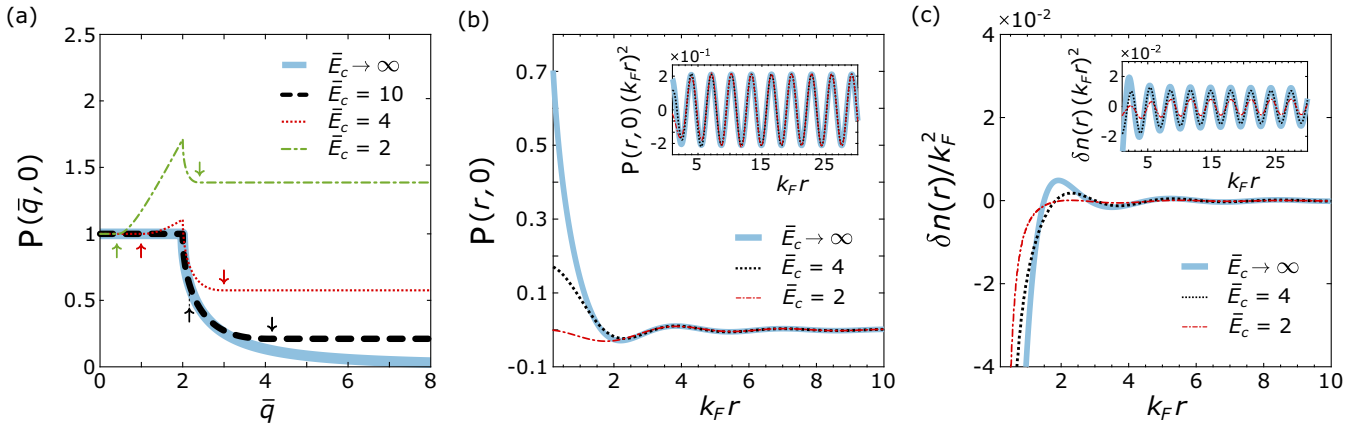


FIG. 4. (a) The static polarizability (normalized to $m/\pi\hbar^2$) vs \bar{q} . The upward (downward) arrows denote $\bar{q} = \bar{k}_c - 1$ ($\bar{q} = \bar{k}_c + 1$). (b) The spatial Fourier transform of the static polarizability (normalized to $m k_F^2/\pi\hbar^2$) as a function of $k_F r$. The inset shows the r^{-2} decay at large distances. (c) Same as (b), for the induced charge density $\delta n(r)$ (in units of $k_F^2 Z e$).

falls off rapidly (with $1/\bar{q}^2$). For FBW-2DEG, however, given that $\bar{q} \geq \bar{k}_c + 1$, the static polarizability is given by

$$P(\bar{q}, 0) = \frac{2m}{\pi\hbar^2} \ln\left(\frac{\bar{E}_c}{\bar{E}_c - 1}\right), \quad (10)$$

i.e., a constant value which depends on the bandwidth and Fermi energy. Moreover, we note that similar to the 2DEG, the polarizability for FBW also has a kink at $\bar{q} = 2$, although its magnitude at $\bar{q} = 2$ increases from that of 2DEG given $\bar{k}_c \leq 3$. It is worthwhile to mention that the increase beyond the 2DEG density of states in the static polarizability for $\bar{k}_c - 1 \leq \bar{q} \leq 2$ can be attributed to the smaller energy denominator in Eq. (2) at $\omega = 0$, which is now limited by the bandwidth. We note in passing that the polarizability kink also implies an observable Kohn anomaly in the FBW-2DEG vibration spectrum [27].

We next discuss the Fourier transform of the static polarizability, given by

$$P(\mathbf{r}, 0) = \frac{1}{4\pi^2} \int d^2q P(q, 0) e^{i\mathbf{q}\cdot\mathbf{r}}, \quad (11)$$

which determines the induced spin density at position \mathbf{r} due a magnetic impurity located at the origin [28]. It also gives the Ruderman-Kittel-Kasuya-Yosida (RKKY) interaction energy between two magnetic impurities, where each impurity interacts with the density induced by the other [29]. From Fig. 4(b), the finite bandwidth does not affect the Friedel oscillations, which appear in the induced spin density (neither the period nor the amplitude) at large distances ($k_F r \gg 1$). However, close to magnetic impurity, the magnitude of the induced spin density is strongly decreased.

We consider next an external charge $n_{\text{ext}}(r) = Ze\delta(r)$ screened by FBW-2DEG, which results in an induced charge density $\delta n(r)$ [10],

$$\delta n(r) = \frac{Ze}{4\pi^2} \int d^2q \left[\frac{1}{\epsilon(q, 0)} - 1 \right] e^{i\mathbf{q}\cdot\mathbf{r}}. \quad (12)$$

According to Fig. 4(c), the induced charge density for FBW follows the same form as the 2DEG, with an oscillatory behavior (with wavelength $\sim \pi/k_F$), which oscillates around

zero and decays with $1/r^2$ at large distances, as verified in the inset of Fig. 4(c). The oscillation amplitude, however, strongly decreases for narrower bandwidth.

IV. COMPARISON WITH TIGHT-BINDING MODELS

Here we verify if the attributes predicted by the toy model are in agreement with the numerical calculations of simple square and hexagonal lattices in tight-binding (TB) approximation. The motive here is to check if simplifications such as the extended flat band at large momenta or the cusp at k_c affect the qualitative picture. In the TB model, assuming one orbital per basis, for the square lattice we have $E_{\mathbf{k}} = -2\gamma[\cos(k_x a) + \cos(k_y a)]$, and for the hexagonal lattice we have $E_{\mathbf{k}} = -2\gamma[\cos(k_x a) + 2\cos(k_x a/2)\cos(k_y a\sqrt{3}/2)]$. Here, a and γ denote, respectively, the lattice constant and the nearest-neighbor hopping amplitude. We set γ to $E_c/8$ ($E_c/9$) for the square (hexagonal) lattice. The panels in Fig. 5 clearly show that the salient features predicted by the toy model are indeed present in the TB calculations. These include the two plasmon branches at large E_c , their merging for narrower bandwidths, negative group velocity which appears close to the Brillouin zone (BZ) edge, the increase in Δ with κ , the kink in the static polarizability, and its evolution with the bandwidth.

We observed in our numerical TB calculations that at rather large E_c [> 7 eV for the parameters in Fig. 5(a)], the second plasmon branch vanishes. To explain this, we note that the singularity in the toy model polarizability, which guarantees large- q plasmon existence, has its origin in flat electronic energy dispersion at large electron momenta [notice Eq. (8), which describes this singularity is obtained for $q \geq k_c + k_F$, where $E_{\mathbf{k}+\mathbf{q}} = E_c$ for all $k \leq k_F$]. For TB models, however, at very large E_c , the electronic band at large electron momenta is quasiflat only in a narrow region close to the BZ edges, and the large- q plasmon branch may vanish depending on the relative positioning of the Fermi level and bandwidth.

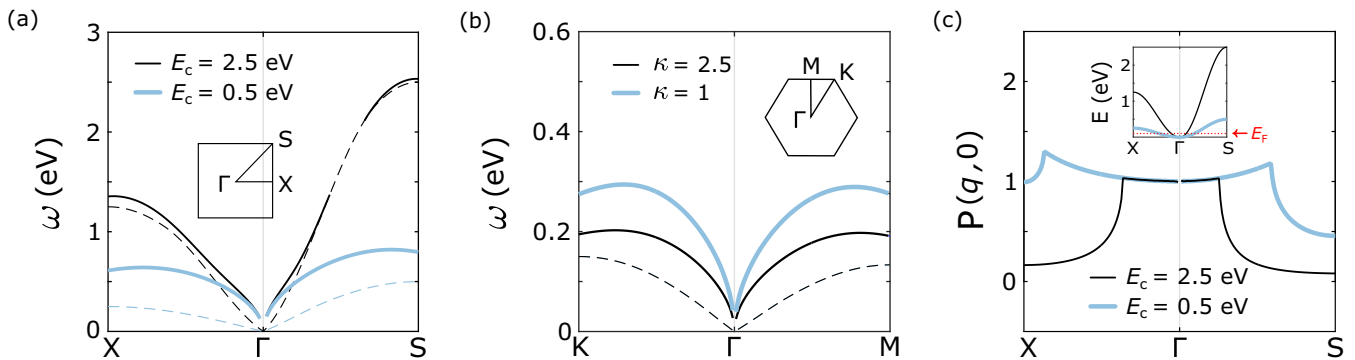


FIG. 5. (a) The plasmon dispersion for the square lattice with $\kappa = 2.5$ and bandwidths $E_c = 2.5$ and 0.5 eV. (b) The plasmon dispersion for a hexagonal lattice with $E_c = 0.15$ eV and $\kappa = 2.5$ and 1 . The dashed lines in (a) and (b) denote the upper boundary of the PHC. (c) The static polarizability (normalized to the density of states at E_F) of the square lattice for $E_c = 2.5$ and 0.5 eV, with the electron energy dispersions depicted in the inset. In all panels, $E_F = 0.1$ eV and $a = 4$ Å.

V. CONCLUSION

In summary, we compute the dielectric function of a 2DEG with finite bandwidth. The dispersing plasmons include modes which can arguably be immune to Landau damping mediated by elastic and inelastic scattering. Moreover, the dispersion has a quasiflat tail which can be extended to large momenta. In the static limit, the FBW polarizability differs from the 2DEG, especially in the large-momenta limit where it saturates to a constant value as opposed to 2DEG where it falls rapidly to zero. Moreover, the static Friedel charge and spin-density oscillations due to a charged or magnetic impurity embedded in FBW-2DEG are computed. The nonanalyticity at $q = 2k_F$ leads to Friedel oscillations with period $\sim \pi/k_F$ decaying as r^{-2} at large distances. The oscillation

amplitudes in induced charge increase with the bandwidth, while the the amplitude remains intact in the induced spin density.

Note added. Recently, we became aware of Ref. [30] in which the authors discuss low-damped plasmonic modes in narrowband electronic systems with the focus on twisted bilayer graphene.

ACKNOWLEDGMENTS

This work has been supported by Spain's MINECO under Grant No. FIS2017-82260-P as well as by the CSIC Research Platform on Quantum Technologies, Grant No. PTI-001. K.K. and T.L. acknowledge support by the National Science Foundation NSF/EFRI Grant No. EFRI-1741660.

- [1] J. Bardeen and W. H. Brattain, *Phys. Rev.* **74**, 230 (1948).
- [2] T. Ando, A. B. Fowler, and F. Stern, *Rev. Mod. Phys.* **54**, 437 (1982).
- [3] B. G. Streetman and S. Banerjee, *Solid State Electronic Devices* (Prentice Hall, New Jersey, 2000).
- [4] K. S. Novoselov, A. K. Geim, S. V. Morozov, D. Jiang, Y. Zhang, S. V. Dubonos, I. V. Grigorieva, and A. A. Firsov, *Science* **306**, 666 (2004).
- [5] S. Das Sarma, S. Adam, E. H. Hwang, and E. Rossi, *Rev. Mod. Phys.* **83**, 407 (2011).
- [6] B. Wunsch, T. Stauber, F. Sols, and F. Guinea, *New J. Phys.* **8**, 318 (2006).
- [7] E. H. Hwang and S. Das Sarma, *Phys. Rev. B* **75**, 205418 (2007).
- [8] A. Scholz, T. Stauber, and J. Schliemann, *Phys. Rev. B* **86**, 195424 (2012).
- [9] T. Low, R. Roldan, H. Wang, F. Xia, P. Avouris, L. M. Moreno, and F. Guinea, *Phys. Rev. Lett.* **113**, 106802 (2014).
- [10] G. Giuliani and G. Vignale, *Quantum Theory of the Electron Liquid* (Cambridge University Press, Cambridge, 2005).
- [11] G. D. Mahan, *Many-particle Physics* (Springer Science & Business Media, New York, 2013).
- [12] M. N. Gjerding, M. Pandey, and K. S. Thygesen, *Nat. Commun.* **8**, 15133 (2017).
- [13] S. Schuwalow, D. Grieger, and F. Lechermann, *Phys. Rev. B* **82**, 035116 (2010).
- [14] P. Hansmann, T. Ayril, L. Vaugier, P. Werner, and S. Biermann, *Phys. Rev. Lett.* **110**, 166401 (2013).
- [15] Z. F. Wang and F. Liu, *Phys. Rev. Lett.* **115**, 026803 (2015).
- [16] T. Stauber, *J. Phys.: Condens. Matter* **26**, 123201 (2014).
- [17] A. Czachor, A. Holas, S. R. Sharma, and K. S. Singwi, *Phys. Rev. B* **25**, 2144 (1982).
- [18] T. Stauber and G. Gómez-Santos, *Phys. Rev. B* **85**, 075410 (2012).
- [19] T. Stauber and H. Kohler, *Nano Lett.* **16**, 6844 (2016).
- [20] V. M. Agranovich and Y. N. Gartstein, *Phys. Usp.* **49**, 1029 (2006).
- [21] H. Shin and S. Fan, *Phys. Rev. Lett.* **96**, 073907 (2006).
- [22] X. Lin and B. Zhang, *arXiv:1909.10885*.
- [23] Y. Jiang, X. Lin, T. Low, B. Zhang, and H. Chen, *Laser Photon. Rev.* **12**, 1800049 (2018).
- [24] J. B. Khurgin and G. Sun, *Appl. Phys. Lett.* **96**, 181102 (2010).

- [25] Y. Hugen, T. Low, W. Zhu, Y. Wu, M. Freitag, X. Li, F. Guinea, P. Avouris, and F. Xia, *Nat. Photon.* **7**, 394 (2013).
- [26] F. Stern, *Phys. Rev. Lett.* **18**, 546 (1967).
- [27] W. Kohn, *Phys. Rev. Lett.* **2**, 393 (1959).
- [28] B. Fischer and M. W. Klein, *Phys. Rev. B* **11**, 2025 (1975).
- [29] M. T. Béal-Monod, *Phys. Rev. B* **36**, 8835 (1987).
- [30] C. Lewandowski and L. Levitov, *Proc. Natl. Acad. Sci.* **116**, 20869 (2019).